APPLIED PHYSICS LETTERS 106, 083105 (2015)

From disk to ring: Aspect ratio control of the magnetoplasmonic response in Au/Co/Au nanostructures fabricated by hole-mask colloidal lithography

Hua Yu Feng (冯华钰),[1] Feng Luo (罗锋),[1] David Meneses-Rodríguez,[2] Gaspar Armelles,[2] and Alfonso Cebollada[2,a)]
[1]*IMDEA Nanoscience, Faraday 9, Ciudad Universitaria de Cantoblanco, 28049 Madrid, Spain*
[2]*IMM-Instituto de Microelectrónica de Madrid (CNM-CSIC), Isaac Newton 8, PTM, E-28760, Tres Cantos, Madrid, Spain*

(Received 22 December 2014; accepted 15 February 2015; published online 24 February 2015)

Morphology tuning of a series of Au/Co/Au nanostructures which gradually evolve from disk to ring allows controlling their optical and magneto-optical spectral responses in the visible and near infrared ranges. This is achieved by the combined use of hole mask colloidal lithography with off-normal deposition and substrate rotation. The morphological parameters responsible for this control, the disk/ring outer diameter and height, are determined by the off-normal deposition angle and the amount of deposited material, respectively. The single dipolar symmetric resonance mode in nanodisk splits into two characteristics, low (symmetric) and high energy (antisymmetric) ring modes. The ring's high energy mode, determined by the rings' section, is basically independent of the deposition angle, while the low energy symmetric mode is basically controlled by the outer diameter/height aspect ratio for both disk-like and ring structures, and therefore allowing a fine tuning of the wavelength position of this resonance. © *2015 AIP Publishing LLC*.
[http://dx.doi.org/10.1063/1.4913621]

In recent years, there has been an increasing interest on the exploration of systems in which surface plasmon resonances and magneto-optical (MO) activity coexist and interact.[1] In these so-called magnetoplasmonic structures, the plasmon resonance control and enhancement of the MO activity has been one of the most intensively studied aspects.[2–7]

Due to the practical interest in general of magnetoplasmonic structures in sensing applications[8,9] as well as telecommunication[10–12] areas, the ability to spectrally tune this plasmon enhanced MO activity (MOA) is of obvious interest. For example, in single resonant magnetoplasmonic nanoelements such as disks[4,7,13,14] and particles,[15] while maintaining all other parameters fixed, their dimensions and aspect ratio are one of the relevant factors that allow controlling the wavelength range at which this enhancement takes place. This can also be achieved and spectrally extended by using multi-resonant systems. For example, in vertically stacked metal/dielectric/metal nanodisk structures[16] both symmetric and antisymmetric modes are excited, obtaining configurations for which large MO activity and low optical losses may be obtained in the same spectral region. Alternatively, magnetoplasmonic nanorings also yield multi-resonant optical and MO responses that extend this effect into the near IR region.[17]

Many of these systems make use the hole mask colloidal lithography (HMCL)[17–19] method for their fabrication, which make it possible to cover cm^2 areas with a large variety of systems of diverse complexity, from simple and multiple nanodisk structures,[14] chiral structures,[20] nanorings,[17] and split ring compositions.[19] The fabrication of these different architectures is basically achieved by different combinations of tilted-angle deposition and rotation in the substrate. For example, normal incidence deposition along with continuous rotation about the surface normal yields nanodisk structures, while similar rotation of the substrate at large enough off-normal deposition angles yields nanoring elements.

Exploiting this great versatility and potential of the HMCL technique, the purpose of this work is to get a deeper insight into the morphology control of the optical and magneto-optical properties of a series of nanostructures that gradually connect two of the most studied systems such as disks and rings.

For this purpose, typical HMCL templates used were fabricated on glass substrates following a standard procedure:[14] Polystyrene spheres (PS) with 124 nm diameter were incubated by PDDA adhesive layer on 200 nm thick PMMA, followed by a 30 nm Au film sputtering over all of the template and tape-stripping to remove all the PS spheres, leaving perforated Au film mask on PMMA. The uncovered part of PMMA layer was etched with oxygen plasma to allow enough space for the deposition of disk or ring structures under the Au film mask. After the deposition process, the whole template was eliminated by lift-off in acetone for 2 h in an ultrasonic bath.

The deposition process was then performed in an ultra-high vacuum system with electron-beam evaporation for Ti and Co, and Knudsen cell for Au. For all the structures, a 1–2 nm Ti layer was deposited first to improve the adhesion of the subsequent Au and Co layers. The deposition rates were 0.02 nm/s for both Ti and Co, and 0.03 nm/s for Au. The rotation speed of the substrate about its surface normal was 3 rpm for all the samples. Additionally, off normal deposition angle was controlled independently to allow fine tuning in the disks and rings fabrication. Sample morphology was characterized by AFM, and optical and MO properties by optical extinction at normal incidence of the light and polar-Kerr spectroscopy in setups described elsewere.[17,21]

a)E-mail: alfonso@imm.cnm.csic.es

In Fig. 1, we sketch the different deposition configurations considered, and representative AFM images of the obtained structures using these configurations. Fig. 1(d) details all the geometrical parameters that determine the lateral dimensions of the obtained structures, namely, D is the diameter of the hole in the Au film mask determined by the diameter of PS sphere, θ is the deposition angle, t is the Au mask layer thickness, and T is the PMMA thickness. At normal deposition ($\theta = 0°$, Figs. 1(a) and 1(e)), the material is deposited in the region below the hole, forming disks. By slightly changing the deposition angle off-normal ($\theta = 8°$, (b) and (f)), opposite deposition angles will produce deposits that overlap in the central region, resulting in over-accumulation of material and larger height in this region with respect to the edge of the nanodisk. Further increase of deposition angle will lead to a situation where a dip in the central part of the disk starts opening up, until deposits produced by opposite angles are just in the limit of physical contact ($\theta = 18°$, (c) and (g)). This case can be considered as the transition between disk and ring formation, from which the central dip becomes a full hollow region. For larger deposition angles ($\theta = 24°$, (d) and (h)), the deposits from opposite angles are away from each other and the substrate rotation about its surface normal leads to ring formation.

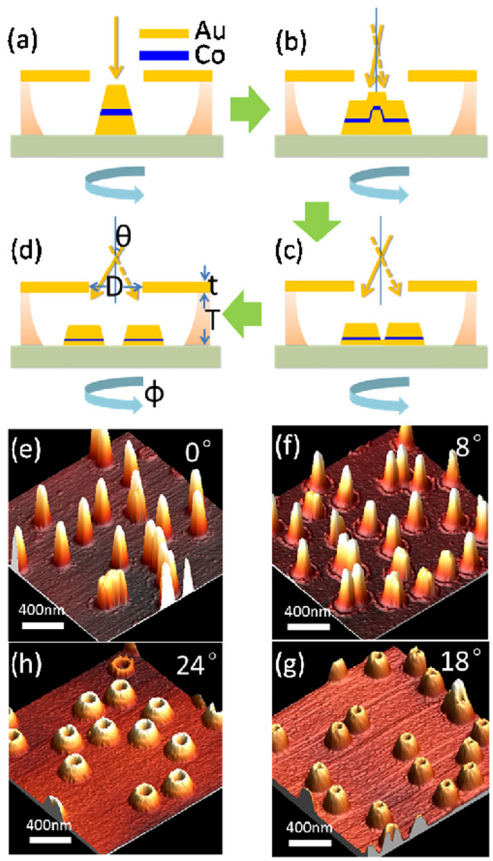

FIG. 1. (a)–(d) Schematic representation of the different deposition geometries for $\theta = 0°$ (a) (disks with flat upper surfaces), 8° (b) (disks with superimposed central regions due to overlapping), 18° (c) (disks with a dip in the central part), and 24° (d) (standard rings). The deposition parameters that define the lateral dimensions of the obtained structures are shown in (d). (e)–(h) Representative AFM images of the structures obtained for $\theta = 0°$ (e), 8° (f), 18° (g), and 24° (h).

Following this procedure, 43 nm Au, 30 nm Co, and 86 nm Au were sequentially deposited at $\theta = 0°$ to obtain the Au/Co/Au trilayer disk. With the purpose of maintaining the amount of plasmonic and ferromagnetic material identical for all the structures, the deposition time of each Au and Co layer for all the other structures was kept the same as that in the $\theta = 0°$ situation, resulting in a gradual reduction of the structure height and increase in the outer diameter due to spatial redistribution of the deposited material as the deposition angle increased. The representative AFM images in Figs. 1(e)–1(h) confirm the described morphological evolution, with a disk shape for 0° and 8°, disks presenting a dip in the central part for 18°, and clear ring shape for 24°.

This morphological evolution becomes even more evident if one compares the AFM profiles of all the structures, which are shown in the left column of Fig. 2. These AFM profiles were obtained by averaging profiles from 10 different nanostructures in each sample. As it can be seen, the overall evolution of the structural shape is clear, being a well-defined disk for 0°, a disk with a taller central part and a shorter edge for 8°, disks with a central dip for 16° and 18°, and ring structures with actually hollow central parts for 20°, 22°, and 24°. The morphological parameters, i.e., outer diameter (D_{out}), height (H) extracted from these profiles, are also listed in Fig. 2, together with the resulting aspect ratio ($AR = D_{out}/H$),[17,22] which exhibits the gradual increase with deposition angle. Additionally, the corresponding parameters calculated using simple geometrical considerations[19,23] and the resulting aspect ratios are also shown in parenthesis, showing excellent agreement with the results extracted from

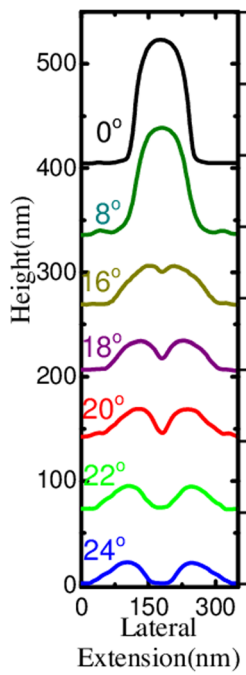

θ (deg.)	Dout (nm)	H (nm)	AR
0	130 (124)	118 (118)	1.1 (1.1)
8	170 (180)	103 (55)	1.7 (3.2)
16	240 (238)	37 (31)	6.5 (7.5)
18	245 (253)	27 (28)	9.1 (8.9)
20	260 (269)	26 (25)	10 (10.5)
22	270 (285)	22 (23)	12.3 (12.2)
24	300 (302)	20 (21)	15 (14.1)

FIG. 2. Left: averaged AFM profiles from 10 different nanostructures in each samples showing clear evolution from disk to ring. Vertical axes are displaced to help the visual inspection. Right: morphological parameters (H for height, D_{out} for outer diameter) obtained from the averaged profiles, and aspect ratio ($AR = D_{out}/H$) for the different deposition angles. In parentheses, the parameters obtained using a simple geometrical calculation according to the deposition parameters shown in Fig. 1(d).

the AFM profiles, except for the 8° sample due to the overlapping deposition effects.

This gradual morphological evolution as a function of the deposition angle while maintaining basically identical amount of plasmonic and MO material has its direct consequence in the optical and MO spectral response of the studied structures. This is illustrated in Fig. 3, where we show the spectral dependence of the extinction (left) and MOA in polar configuration (right) defined as the modulus of the complex Kerr rotation.[16]

As it can be seen for each deposition angle, the spectral dependence of optical extinction and MOA spectra are very similar, confirming the cross correlation between plasmon resonance excitation enhanced electromagnetic field in the MO active component, and the subsequent enhancement of the MOA at resonance.[4,17] Additionally, a clear parallel evolution of both extinction and MOA as a function of deposition angle is also observed: for 0° and 8°, both extinction and MOA spectra exhibit a single resonance. With increasing deposition angles, a new spectral feature begins to appear as a shoulder in the high energy side of the main peak. This additional feature becomes more intense and clearly observable for 20°, 22°, and 24° deposition angles.[17]

These results highlight the optical and MO counterpart of the gradual morphological transition from disk to ring obtained by modifying the deposition parameters: The single mode feature observed for disk structures (0° and 8°) corresponds to the excitation of the disk dipolar resonance mode, the low extinction and MOA values observed relative to the rest of deposition angles being simply due to the low aspect ratios and therefore small dipole moments.[4,22] On the other extreme of the series of structures, the bimodal behavior for ring (20°, 22°, and 24°) can be interpreted in terms of the disk-hole dipole hybridization model,[17] inducing a symmetric dipolar mode in the low-energy range and an antisymmetric dipolar mode in the high-energy range. The high energy mode may also have contributions from higher order modes, but for normal incidence, this contribution is expected to be small.[24,25] On the other hand, the intermediate structures grown at 16° and 18° corresponding to disks with a central dip show an intermediate behavior, with a main resonance in low energy range and a very small shoulder in high energy range.

Up to this point, it is evident that the mode for disk structures and the low energy mode observed for the rings share a common dipolar symmetric nature and the spectral shift of these modes occur in a gradual fashion all the way when transiting from disk to ring structures. Since the relevant parameter governing this feature in disk structures is the aspect ratio,[17,22] in Fig. 4 we have plotted the wavelength position for both optical and MO modes versus the corresponding aspect ratios. As it can be seen, the low energy optical and MO modes for both disks and rings gradually red shift in an identical linear fashion with increasing aspect ratio, from 650 nm for pure disk structures up to 1200 nm for pure rings. This highlights the clear "disk-like" nature of the low energy mode, whose spectral position is governed by the aspect ratio of the structure, with very little or almost absent effect of the hole. On the other hand, in Fig. 4 the high energy (HE) mode position is also shown for the ring structures, which are the only ones where this mode is observed. In this case, its position hardly depends on the aspect ratio, as expected since it basically depends on the ring section.[26]

In summary, we have shown how the HMCL technique allows finely controlling the morphology and aspect ratio of Au/Co/Au magnetoplasmonic structures that gradually evolve from disk to ring. As a consequence, a gradual evolution of the optical and MO spectral responses is also observed, allowing an accurate control on the spectral position of the desired MO features by simple structural design.

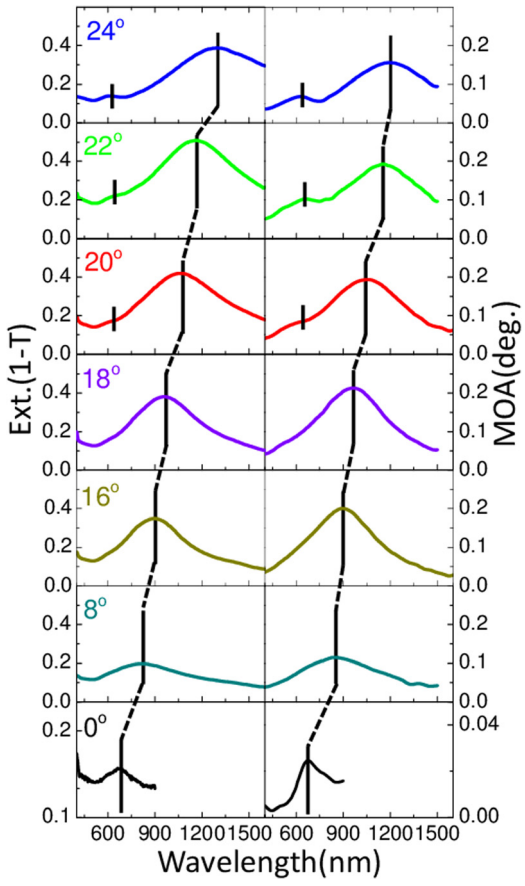

FIG. 3. Optical extinction (left) and polar MO activity (right) spectra showing unimodal to bimodal evolution from disk to ring. Black lines are guides to the eye showing the gradual spectral shift behavior of the low energy (LE) mode, clearly observable for all the structures. The high energy modes evident for 20°–24° deposition angles are also marked with black bars. Note the different scales for spectra at 0° deposition angle.

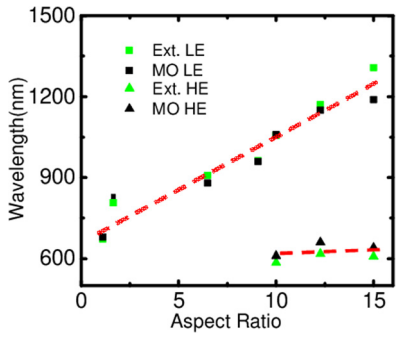

FIG. 4. Low and high energy (LE and HE) optical and MO resonance wavelength position as a function of the aspect ratio (dashed lines are guides to the eye).

This control is obtained in the low energy mode, of both disk and ring structures. This disk-like nature of this mode is confirmed by the almost absent effect of the hole on it, with a linear dependence of its spectral position on the aspect ratio, regardless either disk or ring structures. The high energy mode is governed by the rings section, determined by the template hole diameter, and therefore its spectral position remains unaltered for all the structures where it is present. These findings may be useful in the detailed design of magnetoplasmonic structures whose MO response in specific spectral ranges may be desired, in sensing or telecommunication applications.

Funding from Spanish Ministry of Economy and Competitiveness through Grants "FUNCOAT" CONSOLIDER CSD2008–00023 and MAPS MAT2011–29194-C02–01are acknowledged. H. Y. Feng thanks the funding from CSC (Chinese Scholarship Council), Grant No. 201206220112. F. Luo would like to acknowledge the support of NSFC (Nos. 51002003 and 11090332) as well as Ramon y Cajal grant RYC-2012-11954.

[1]G. Armelles, A. Cebollada, A. García-Martín, and M. U. González, Adv. Opt. Mater. **1**, 10 (2013).
[2]V. I. Safarov, V. A. Kosobukin, C. Hermann, G. Lampel, J. Peretti, and C. Marlière, Phys. Rev. Lett. **73**, 3584 (1994).
[3]A. A. Grunin, A. G. Zhdanov, A. A. Ezhov, E. A. Ganshina, and A. A. Fedyanin, Appl. Phys. Lett. **97**, 261908 (2010).
[4]J. B. González-Díaz, A. García-Martín, J. M. García-Martín, A. Cebollada, G. Armelles, B. Sepúlveda, Y. Alaverdyan, and M. Käll, Small **4**, 202 (2008).
[5]L. Wang, C. Clavero, Z. Huba, K. J. Carroll, E. E. Carpenter, D. Gu, and R. A. Lukaszew, Nano Lett. **11**, 1237 (2011).
[6]J. Y. Chin, T. Steinle, T. Wehlus, D. Dregely, T. Weiss, V. I. Belotelov, B. Stritzker, and H. Giessen, Nat. Commun. **4**, 1599 (2013).
[7]G. X. Du, T. Mori, M. Suzuki, S. Saito, H. Fukuda, and M. Takahashi, J. Appl. Phys. **107**, 09A928 (2010).
[8]B. Sepúlveda, A. Calle, L. M. Lechuga, and G. Armelles, Opt. Lett. **31**, 1085 (2006).
[9]M. G. Manera, G. Montagna, E. Ferreiro-Vila, L. González-García, J. R. Sánchez-Valencia, A. R. González-Elipe, A. Cebollada, J. M. García-Martín, G. Armelles, and R. Rella, J. Mater. Chem. **21**, 16049 (2011).
[10]B. Sepúlveda, L. M. Lechuga, and G. Armelles, J. Lightwave Technol. **24**, 945 (2006).
[11]M. Vanwolleghem, W. Van Parys, D. Van Thourhout, R. Baets, F. Lelarge, O. Gauthier-Lafaye, B. Thedrez, R. Wirix-Speetjens, and L. Lagae, Appl. Phys. Lett. **85**, 3980 (2004).
[12]B. K. Chau, S. Irvine, and A. Elezzabi, IEEE J. Quantum Electron. **40**, 571 (2004).
[13]V. Bonanni, S. Bonetti, T. Pakizeh, Z. Pirzadeh, J. Chen, J. Nogués, P. Vavassori, R. Hillenbrand, J. Åkerman, and A. Dmitriev, Nano Lett. **11**, 5333 (2011).
[14]D. Meneses-Rodríguez, E. Ferreiro-Vila, P. Prieto, J. Anguita, M. U. González, J. M. García-Martín, A. Cebollada, A. García-Martín, and G. Armelles, Small **7**, 3317 (2011).
[15]L. Wang, K. Yang, C. Clavero, A. Nelson, K. Carroll, E. Carpenter, and R. A. Lukaszew, J. Appl. Phys. **107**, 09B303 (2010).
[16]J. C. Banthí, D. Meneses-Rodríguez, F. García, M. U. González, A. García-Martín, and G. Armelles, Adv. Mater. **24**, OP36 (2012).
[17]H. Y. Feng, F. Luo, R. Kekesi, D. Granados, D. Meneses-Rodríguez, J. M. García, A. García-Martín, G. Armelles, and A. Cebollada, Adv. Opt. Mater. **2**, 612 (2014).
[18]H. Fredriksson, Y. Alaverdyan, A. Dmitriev, C. Langhammer, D. S. Sutherland, M. Zäch, and B. Kasemo, Adv. Mater. **19**, 4297 (2007).
[19]S. Cataldo, J. Zhao, F. Neubrech, B. Frank, C. Zhang, P. V. Braun, and H. Giessen, ACS Nano **6**, 979 (2012).
[20]B. Frank, X. Yin, M. Schäferling, J. Zhao, S. M. Hein, P. V. Braun, and H. Giessen, ACS Nano **7**, 6321 (2013).
[21]W. S. Kim, M. Aderholz, and W. Kleemann, Meas. Sci. Technol. **4**, 1275 (1993).
[22]P. Hanarp, M. Käll, and D. S. Sutherland, J. Phys. Chem. B **107**, 5768 (2003).
[23]S. Syrenova, C. Wadell, and C. Langhammer, Nano Lett. **14**, 2655 (2014).
[24]R. Vogelgesang, J. Dorfmüller, R. Esteban, R. T. Weitz, A. Dmitriev, and K. Kern, Phys. Status Solidi B **245**, 2255 (2008).
[25]F. Hao, E. M. Larsson, T. A. Ali, D. S. Sutherland, and P. Nordlander, Chem. Phys. Lett. **458**, 262 (2008).
[26]J. Ye, P. V. Dorpe, L. Lagae, G. Maes, and G. Borghs, Nanotechnology **20**, 465203 (2009).